

Spectroscopy of the superdeformed band in ^{196}Pb

E. F. Moore,¹ Y. Liang,^{2,*} R. V. F. Janssens,² M. P. Carpenter,² I. Ahmad,² I. G. Bearden,³ P. J. Daly,³ M. W. Drigert,⁴ B. Fornal,³ U. Garg,⁵ Z. W. Grabowski,³ H. L. Harrington,¹ R. G. Henry,² T. L. Khoo,² T. Lauritsen,² R. H. Mayer,³ D. Nisius,³ W. Reviol,^{5,†} and M. Sferrazza³

¹North Carolina State University, Raleigh, North Carolina 27695

and Triangle Universities Nuclear Laboratory, Durham, North Carolina 27708

²Argonne National Laboratory, Argonne, Illinois 60439

³Purdue University, West Lafayette, Indiana 47907

⁴Idaho National Engineering Laboratory, EG&G Idaho Inc., Idaho Falls, Idaho 83415

⁵University of Notre Dame, Notre Dame, Indiana 46556

(Received 2 July 1993)

The superdeformed band in ^{196}Pb has been studied extensively using the reaction $^{170}\text{Er}(^{30}\text{Si},4n)$ at beam energies of 142, 146, and 151 MeV. New transitions have been added at the top and bottom of the previously known band. Gamma-ray directional correlations were measured for most of the transitions in the band verifying the expected stretched $E2$ character. The collectivity of the band has been measured using the Doppler shift attenuation method yielding an intrinsic quadrupole moment Q_0 of $18.3 \pm 3.0 e b$, in good agreement with theoretical predictions. The variations of the dynamic moment of inertia $\mathcal{J}^{(2)}$ as a function of the rotational frequency $\hbar\omega$ have been studied and compared with cranked shell model calculations. The dependence of $\mathcal{J}^{(2)}$ on mass for superdeformed bands in the Pb isotopes is also investigated.

PACS number(s): 21.10.Re, 21.10.Ft, 23.20.Lv, 27.80.+w

I. INTRODUCTION

The region of superdeformed nuclei with mass $A \sim 190$ has been studied extensively over the last few years. Following the original discovery in ^{191}Hg [1] of a rotational band of 12 transitions with an average energy spacing of 37 keV, an average dynamic moment of inertia $\mathcal{J}^{(2)}$ of $110\hbar^2 \text{ MeV}^{-1}$, and an average quadrupole moment of $18 \pm 3 e b$, several other bands with similar properties were found in the neighboring nuclei. In fact, superdeformed bands have now been identified in all Hg isotopes with mass $189 \leq A \leq 194$, in the Tl isotopes with mass $191 \leq A \leq 195$, and in the even-even Pb isotopes with $192 \leq A \leq 198$ (see Ref. [2] for a recent review). In many instances, several superdeformed bands have been observed in a single nucleus. These experimental observations confirm theoretical calculations [3–9] indicating that a region of superdeformation should occur near $A = 190$ which is brought about by the presence of large shell gaps for $Z=80$ and $N=112$, at deformations corresponding to a 1.65:1 axis ratio ($\beta_2 \sim 0.5$). In all the calculations, these gaps are found to exist even at the lowest spins.

Superdeformed bands are usually identified in the γ -ray spectra by the presence of a sequence of transitions almost equally spaced in energy. Typically, this signature

is fairly unambiguous. Nevertheless, it remains important to establish the deformation directly through lifetime measurements. This is especially true in the $A \sim 190$ region, in view of the observation that, in the vast majority of these superdeformed bands, the moment of inertia $\mathcal{J}^{(2)}$ rises smoothly with the rotational frequency $\hbar\omega$. A change in deformation with rotational frequency is a possible, albeit unlikely, explanation for this effect. Lifetime measurements have thus far been performed with the Doppler shift attenuation method (DSAM) for superdeformed bands in $^{190,191,192}\text{Hg}$ [1,10–12] and more recently in ^{194}Pb [13].

Here we report on a new experimental study of superdeformation in ^{196}Pb . The observation of superdeformation in this nucleus was originally reported by Brinkman *et al.* [14]. The same group later performed a more detailed study [15] where, in particular, the isotopic assignment of the superdeformed band to ^{196}Pb was confirmed via the cross bombardments $^{176}\text{Yb}(^{26}\text{Mg},xn)$ and $^{176}\text{Yb}(^{24}\text{Mg},xn)$. In the present work, data were accumulated with thin and backed targets in order to search for additional superdeformed bands and to characterize the known band further by measuring the associated deformation and by extending the sequence of transitions towards higher rotational frequency. While no new superdeformed bands were found in this nucleus, it was possible to characterize the highest transitions in the superdeformed band with more accuracy and to extend the sequence by two transitions. The latter turn out to be important when the evolution of the $\mathcal{J}^{(2)}$ moment of inertia with $\hbar\omega$ is discussed. The value of the measured quadrupole moment has been compared with those reported for the other superdeformed bands of the region as well as with the results of various calculations. A com-

*Present address: Dept. of Radiology, Indiana University Medical Center, Indianapolis, IN 46202.

†Present address: Physics Dept., University of Tennessee, Knoxville, TN 37996.

parison of the evolution of the moments of inertia with mass was also performed.

The experimental techniques are described briefly in Sec. II. Section III introduces the new results obtained in the present studies. These results are then interpreted in Sec. IV which is followed by a brief conclusion. Spectroscopic data required for superdeformation studies are usually of such quality that a significant improvement in the general knowledge of the nucleus under investigation is possible. This was certainly the case here: The discovery of three collective bands of $M1$ transitions in ^{196}Pb has recently been reported [16], and a detailed discussion of extended level schemes for ^{196}Pb and ^{195}Pb is in preparation [17].

II. EXPERIMENT

Two experiments to study the superdeformed (SD) band in ^{196}Pb were performed at Argonne National Laboratory using the Argonne superconducting linear accelerator ATLAS. Details of the experiments are given below.

A. Thin-target measurements

In the first experiment, beams of ^{30}Si ions were used at 142, 146, and 151 MeV to populate high-spin states in the nucleus ^{196}Pb via the $^{170}\text{Er}(^{30}\text{Si},4n)$ reaction. The target consisted of two $500\ \mu\text{g}/\text{cm}^2$ ^{170}Er self-supporting foils isotopically enriched to 95%. The evaporation residues were allowed to recoil into a vacuum and were stopped in a thick Pb foil located about 10 cm from the target, well away from the center of the γ -ray detection system and out of the view of the Ge detectors.

The γ rays were detected in the Argonne-Notre Dame BGO γ -ray facility, which consists of 12 Compton suppressed Ge spectrometers (CSG's) surrounding an inner array of 50 hexagonal bismuth germanate (BGO) elements. The CSG's are positioned at angles of 34.5° , 90° , and 145.5° to the beam direction, with four detectors at each angle. The target to detector distances are 18 cm. Energy and efficiency calibrations of the CSG's were carried out by accumulating spectra from ^{152}Eu , ^{56}Co , ^{182}Ta , and ^{243}Am sources.

At each of the three beam energies, data were accumulated in both "singles" and coincidence mode: In the "singles" mode, γ -ray energies measured in individual CSG's were recorded, together with the number of array elements firing in prompt coincidence with the beam (fold) and the total γ -ray energy deposited in the array (sum energy). In the coincidence mode, only those events satisfying the hardware requirements that a minimum of two CSG's and four or more (three or more for the 142 MeV measurement) BGO elements fire in prompt coincidence were accepted and stored event by event on magnetic tape for subsequent off-line analysis. In addition to the energy and time information for the CSG's, the γ -ray sum energy, prompt, and delayed fold, and the hit pattern of the array were also recorded.

The singles data were used as an "unbiased" measure

of the relative population of the SD band with respect to the ^{196}Pb reaction channel as well as a check of the ratio of $4n$ to $3n$ and $5n$ reaction strengths as a function of beam energy. The singles data were also used to determine the fold and sum-energy distributions associated with known transitions in the various evaporation channels. This information was later used in the off-line analysis to enhance channel selection in the production of γ - γ coincidence matrices by placing appropriate gates on the array parameters. In coincidence mode, approximately 66, 147, and 81×10^6 events were recorded at the beam energies of 142, 146, and 151 MeV, respectively.

B. Backed-target measurements

The DSAM experiment was performed with the same reaction and under similar experimental conditions as those described above. In this case, the target consisted of $1.0\ \text{mg}/\text{cm}^2$ of ^{170}Er evaporated on a $24\ \text{mg}/\text{cm}^2$ thick lead backing. From an initial recoil velocity of $v = 0.015c$, the recoiling Pb nuclei were slowed down in the target and backing before coming to a complete rest in the backing. The γ rays emitted from states with very short effective lifetimes are expected to show a large fraction of the full Doppler shift in the detectors at forward and backward angles. On the other hand, those γ rays emitted from states having effective lifetimes of 1–2 ps or more (comparable to the stopping time of the recoils in the target) should exhibit no Doppler shift.

The experiment was carried out at a beam energy of 142 MeV. This choice of beam energy was determined from the analysis of the excitation function: The population of the SD band was found to be "optimum" at this energy; i.e., it is at this beam energy that it is possible to obtain the largest number of coincidence spectra, gated on SD γ rays, free of contaminants. Again, a threshold of two or more CSG's and a minimum of three BGO elements firing in prompt coincidence were required for the events to be recorded. As was the case in the thin-target experiment, the energy and timing information from the CSG's and the fold and sum energy derived from the array were written on tape. A total of 72×10^6 coincidence events were stored and analyzed.

In the off-line analysis, γ - γ coincidence matrices were created for all CSG angle combinations. The condition of BGO fold ≥ 9 was required during the sorting process in order to enhance the relative intensity of the $4n$ channel in the matrices. The total number of coincident events satisfying this condition amounted to $\sim 30 \times 10^6$.

III. ANALYSIS AND RESULTS

A. γ - γ coincidences and directional correlation ratios

The thin-target coincidence data were corrected for the Doppler shift and, after proper subtraction of random

and pileup events, were sorted into 2048×2048 channel matrices. At each beam energy, individual matrices were constructed for the various CSG angle combinations, as was a “summed” matrix containing all angle combinations. The BGO fold requirements used in the sorting process were adjusted to compensate for shifts in the fold distributions as a function of beam energy.

The spectrum presented in Fig. 1 is the sum of spectra in coincidence with the cleanest coincidence gates in the SD band. The spectra were obtained from the sum of the 142 MeV and 146 MeV thin-target data sets, under the requirement of a fold of 12 or more in the array. Table I lists the γ -ray energies and intensities extracted from these data. The SD transitions previously reported [14,15] are all present. A transition at 170 keV, recently reported by Henry *et al.* [18], is also evident. This γ ray is interpreted as the lowest member of the SD band. New transitions at 645 and 689 keV can clearly be seen in the present data. They extend the SD band by two transitions. There is also a weak 129 keV γ ray present in the coincidence spectra gated on the SD transitions. Due to the very low intensity of this γ ray, it was not possible to determine whether this transition is a member of the SD band or is associated with the feeding of the near-yrast states (decay out). The relationship of the energy of this γ ray to those of the SD band members suggests that this transition is not a member of the band. In addition, the intensity of this γ ray is stronger than that of the 170 keV transition (after corrections are made for internal conversion and detector efficiency), again suggesting that this transition is associated with the feeding of yrast states.

Figure 2 presents the intensity pattern for the transitions in the SD band as derived from the analysis of the thin-target data. This intensity pattern exhibits characteristics similar to those seen in other SD bands of this mass region; i.e., the feeding occurs over the highest six transitions in the band, the flux remains essentially con-

stant over the next six transitions, and the decay out occurs rapidly over the lowest two transitions. An overall intensity for the SD band of 1.3% of the $4n$ channel was estimated from the backed-target singles data. The presence of several long-lived isomers in the low-spin level scheme of ^{196}Pb [17,19] prevents the observation of yrast and near-yrast transitions in prompt coincidence with the SD band. As was the case in the previous experimental studies [14,15], the population of the SD band was found to exhibit the same beam energy dependence as the $4n$ channel, consistent with the assignment of this band to ^{196}Pb . The data were carefully examined for the presence of other SD bands by the inspection of one-dimensional gated coincidence spectra and two-dimensional searches for grid patterns in the γ - γ coincidence matrices. No other SD bands were observed within our estimated sensitivity of the order of 0.4% of the ^{196}Pb total yield.

The $E2$ multipolarity of the members of the band was established from the γ -ray directional correlations. The experimental directional correlation (DCO) ratios were constructed from the angle-sorted matrices as follows:

$$R(\text{DCO}) = \frac{I_{\gamma}(34.5^{\circ}, 145.5^{\circ}; \text{gate} = 34.5^{\circ}, 145.5^{\circ})}{I_{\gamma}(90.0^{\circ}; \text{gate} = 34.5^{\circ}, 145.5^{\circ})},$$

where I_{γ} is the coincident intensity of the γ ray of interest, measured at the specified angle, and the gating transition is always at an angle of 34.5° or 145.5° . This method has the advantage that the DCO ratio is independent of the multipolarity of the gating transition [20]. The DCO ratios, extracted for members of the SD band, are presented in Table I. The values cluster nicely between 1.3 and 1.4, consistent with the DCO ratios of known yrast $E2$ transitions in ^{196}Pb .

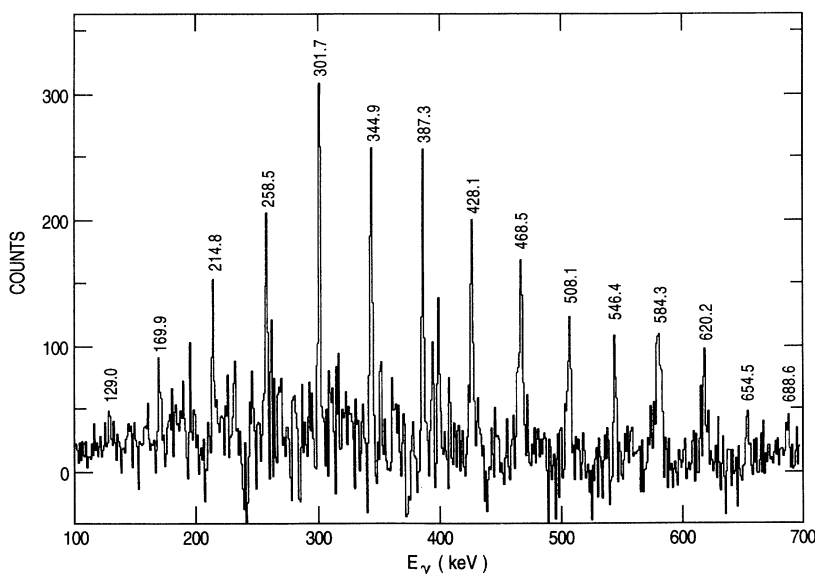


FIG. 1. γ -ray spectrum obtained by summing spectra in coincidence with the 214, 257, and 387 keV transitions. The spectrum represents the sum of thin-target data taken at beam energies of 142 and 146 MeV, as discussed in the text. The energies of the SD transitions are indicated. Note that the 129 keV line is not considered to be a member of the band, but is most likely associated with the decay process (see text for details).

TABLE I. Summary of results for the SD band in ^{196}Pb . The γ -ray energies, intensities corrected for internal conversion and detection efficiency (normalized to 100 for the 345 keV transition), and DCO ratios were extracted from the thin-target measurement. The fractions of the full Doppler shift $F(\tau)$, for $E_\gamma \leq 345$ keV, are all equal to zero. Except where indicated, the mean lifetime values were calculated, following correction for internal conversion, from the Q_0 value of 18.3 e b obtained from a fit to the $F(\tau)$ data (see text for details).

E_γ (keV)	I_γ	$R(\text{DCO})$	$F(\tau)$	τ (ps)	Q_0 (e b)
169.9(3)	19(3)			31.5	18.3(3.0)
214.8(2)	49(6)	1.37(28)		12.3	18.3 (3.0)
258.5(2)	89(11)	1.35(19)		5.32	18.3 (3.0)
301.7(2)	98(13)	1.32(15)		2.56	18.3 (3.0)
344.9(2)	100(8)	1.38(13)		1.34	18.3 (3.0)
387.3(2)	94(8)	1.40(12)	0.02(4)	0.76	18.3 (3.0)
428.1(2)	91(12)	1.28(15)	0.09(8)	0.46	18.3 (3.0)
468.5(2)	90(10)	1.37(17)	0.17(7)	0.33(15) ^a	17.3(^{+6.1} _{-3.0}) ^a
508.1(2)	76(8)	1.43(22)	0.40(12)	0.18(⁺⁴ ₋₈) ^a	19.1(^{+6.5} _{-1.8}) ^a
546.4(2)	53(9)	1.39(25)	0.57(10)	0.12(⁺⁷ ₋₃) ^a	19.6(^{+3.0} _{-4.0}) ^a
584.3(2)	41(6)	1.25(25)	0.77(8)	0.10	18.3(3.0)
620.2(2)	36(8)	1.29(35)	0.76(7)	0.07	18.3(3.0)
654.5(3)	15(3)		0.83(10)	0.06	18.3(3.0)
688.6(3)	14(4)		0.91(7)	0.04	18.3(3.0)

^aDerived from the line-shape analysis as described in the text.

B. DSAM measurement

In the analysis of the backed-target data, spectra in coincidence with low-lying SD transitions, which decay after the residues have stopped in the Pb backing, were produced from the angle-sorted matrices. The spectra gated on the 214, 257, and 387 keV γ rays were found to be the cleanest and were summed together. Information on the lifetimes of states in the SD band was extracted from these spectra in a two-step approach. First, a centroid-shift analysis was performed on the entire band, under the assumption of a constant value of the quadrupole moment. Subsequently, a line-shape analysis was performed for those transitions having contaminant free, statistically significant line shapes.

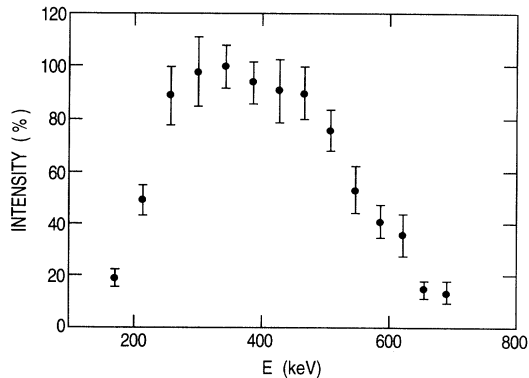


FIG. 2. Relative intensity of the γ rays in the superdeformed band of ^{196}Pb as measured in the thin-target experiment. The data are normalized to the intensity of the 345 keV γ ray, which was taken to be 100%.

In each step of the analysis, the experimental Doppler shifts were compared to corresponding values calculated with the computer code LILIFI [21]. The electronic and nuclear components of the stopping power were calculated with the code TRIM85 [22], which uses the most recent and complete evaluation of existing stopping-power data. The slowing down history of 10^4 recoiling Pb ions in both the target and backing were traced in a Monte Carlo simulation. The effects of lateral and longitudinal straggling were included, as were corrections for the finite solid angle of the Ge detectors and the positional dependence of their efficiencies.

The value of the centroid shift for each Doppler-shifted transition, presented in Table I, was extracted from the difference in the centroid energy as measured in the forward and backward Ge detectors. Figure 3 presents the experimentally measured fractions of the full Doppler shift $F(\tau)$ as a function of γ -ray energy. The curves represent the calculated values of F for various quadrupole moment Q_0 values, under the assumption of constant deformation throughout the entire band. The calculations were performed under the assumption that the side feeding into each state consists of a rotational cascade with effective lifetimes equal to those in the SD band itself, as was found to be the case to a good approximation in the SD band in ^{192}Hg [12]. A chi-squared fit to the data yields a best fit value of 18.3 ± 2.2 e b. When the uncertainties in the slowing down processes and side-feeding lifetimes and intensities are taken into account, error bars of ± 3.0 e b are obtained. From this Q_0 value, the mean lifetimes of the states in the SD band were calculated using the rotational formula, after applying a correction for internal conversion. Table I lists the lifetime values calculated in this manner for all transitions which were not analyzed by means of line-shape fitting.

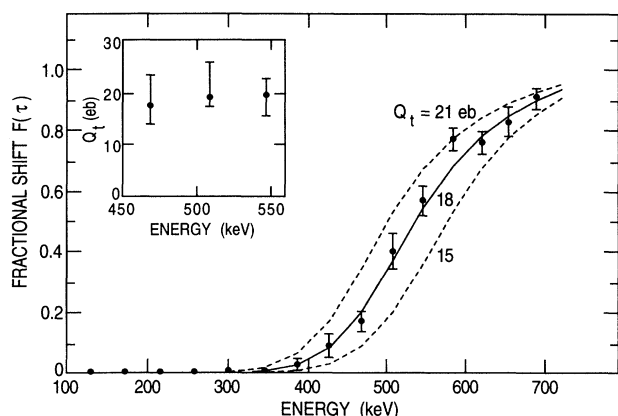


FIG. 3. Measured fraction of the full Doppler shift $F(\tau)$ for transitions in the superdeformed band of ^{196}Pb . The solid line corresponds to the calculated shift for a Q_0 value of 18 eb and the dashed lines are for Q_0 values of 15 and 21 eb. Inset: Quadrupole moment values extracted from line-shape fits to the 468, 508, and 546 keV transitions (see text for details).

The inset to Fig. 3 shows the results of the line-shape analysis carried out for the 546, 508, and 468 keV transitions. Figure 4 presents the line-shape fits to spectra measured in the backward detectors. In the line-shape fitting process, the lifetime values for the higher-lying states were taken from the results of the centroid-shift

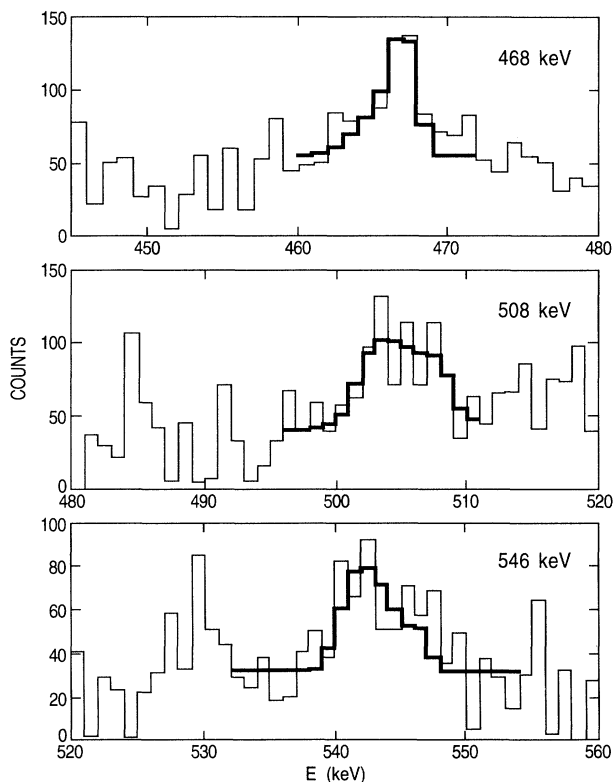


FIG. 4. Examples of line-shape fits (thick line) to the 468, 508, and 546 keV transitions as measured in the detectors at backward angles. The data are represented by the thin lines.

analysis described above. The calculations include (i) the decay within the SD band (with measured γ -ray energies and intensities), (ii) a set of precursor transitions (with the same moment of inertia) preceding the highest known SD transition, and (iii) side feeding into each state, approximated by a single rotational cascade of five transitions. The lifetimes within the feeder bands were controlled by a single parameter $(Q_0^2/\mathcal{J}_{\text{SF}}^{(2)5})_{\text{SF}}$, where $(Q_0)_{\text{SF}}$ and $\mathcal{J}_{\text{SF}}^{(2)}$ are the effective quadrupole moments and moments of inertia, respectively, for the side-feeding cascades. The procedure is discussed in detail in Ref. [23].

As illustrated in Fig. 4, the measured line shapes are reproduced reasonably well in the fitting process. The mean lifetimes extracted from the fits are listed in Table I. The error bars include statistical uncertainties as well as uncertainties due to the treatment of side-feeding lifetimes and intensities. Due to the relatively low statistical accuracy of the present data and the relatively small contribution of side feeding in the region of the band covered by the transitions that were analyzed, it was not possible to extract meaningful information on the effective lifetimes of the side-feeding “bands” as was done in the case of the SD band in ^{192}Hg [12].

After correction for internal conversion, the lifetime values were transformed into transition quadrupole moments using the rotational band formula

$$Q_t(I) = (1.22 \langle I020 | I - 20 \rangle^2 \tau E_\gamma^5)^{-1/2},$$

assuming that the lowest observed member in the band corresponds to the $I = 6 \rightarrow 4$ transition and that the band-head spin is zero ($K = 0$). The resulting Q_t values are shown in the inset to Fig. 3. While the error bars are large, the Q_t values obtained from the individual line-shape fits are consistent with the results of the centroid-shift analysis of the entire band, thereby reinforcing our confidence in the analysis. The lifetime analysis indicates that the deformation in the band remains constant, within error bars, as was found to be the case in lifetime measurements carried out on the SD bands in ^{192}Hg [12] and ^{194}Pb [13]. In the following section, the implications of these measurements concerning the deformation in the SD bands and the relationship with the $\mathcal{J}^{(2)}$ moment of inertia will be discussed within the context of theoretical calculations.

IV. DISCUSSION

For over 20 years now, theoretical calculations have predicted the occurrence of superdeformed shapes in nuclei located in various “islands” of the periodic chart. Following the discovery of a discrete line SD band in ^{152}Dy [24], and later in ^{191}Hg [1], numerous groups have carried out detailed calculations which attempt to reproduce the properties of the known bands and predict where new regions of SD nuclei may be found. With such a large number of calculations now available, it is informative to compare some of the results of theory to the experimen-

tally measured properties of the SD band of ^{196}Pb , as well as to those of other SD bands in the $A \sim 190$ mass region.

A. Deformation parameters

Generally speaking, theoretical calculations provide information on a variety of properties of SD bands, including deformation, excitation energy, spin, and parity. On the other hand, experimental difficulties tend to restrict the measurable properties to γ -ray energies, intensities, and, in a few favorable cases, lifetimes. Therefore, the quantities most readily available for a comparison with theory are the dynamic moments of inertia $\mathcal{J}^{(2)}$, derived from the γ -ray energies, and the intrinsic quadrupole moments Q_0 , derived from the measured lifetimes.

Table II compares the measured quadrupole moments for all SD bands of the mass 190 region for which this information is currently available with the results of calculations based on a variety of theoretical models predicting the location of the superdeformed minima in deformation space. In cases where the evolution of the SD minimum in deformation space is calculated as a function of $\hbar\omega$, average values of the deformation parameters are listed in the table. The quadrupole moment values presented for the calculations of Chasman [3] were derived from the corresponding deformation parameters using the formula of Löbner *et al.* [25]; those given for the calculations of Satała were derived using the prescription given by Nazarewicz *et al.* [26]. The other calculated quadrupole moments were taken directly from the corresponding references.

A close inspection of Table II indicates that the agreement between experiment and theory is quite satisfactory; i.e., calculations using techniques as different as the cranked Strutinsky approach [3,5], the Hartree-Fock + BCS approximation [6,8,9], and the generator coordinate method [27] all indicate very large deformations, in agreement with the data. This observation holds for every SD band in the $A \sim 190$ region for which lifetime data are available.

It is worth pointing out that most of the lifetime data of Table II have been analyzed in the same way. In fact, for five of the seven measurements, the same analysis methods, stopping-power parametrizations, and computer codes have been used. As systematic effects are an important contribution to the experimental uncertainties, it is possible that the differences between the Q_0 values for $^{190,191}\text{Hg}$ and ^{192}Hg as well as those noted between ^{194}Pb and ^{196}Pb have some significance. The data may suggest that the SD quadrupole moments reach a maximum value for $N = 112$ in both the Hg and Pb isotopic chains. It is for this neutron number that the large shell gap responsible in part for the occurrence of superdeformation in this mass region is calculated to occur. We note that the same trend in the evolution of Q_0 with N is present in the cranked Strutinsky calculations of Refs. [3,5]. The situation is not as clear for the other calculations (Table II), even though the values of the quadrupole moment also agree within the errors with the measured quantities.

Another possible experimental indication for small differences in the deformations associated with various SD bands might come from the respective values of $\mathcal{J}^{(2)}$ at

TABLE II. Summary of results for calculated deformation parameters and quadrupole moments, and measured quadrupole moments in the SD bands of selected Hg and Pb isotopes. The calculated results are taken from Chasman [3], Satała *et al.* [5], Meyer *et al.* [9], Krieger *et al.* [8], and Bonche *et al.* [6,27]. The β_2 and β_4 values presented for the calculations of Chasman were derived from the values of the ν_2 and ν_4 deformation parameters given in the original paper. All quadrupole moment values are in e b.

Nucleus <i>A</i>	Expt. <i>Q</i> ₀	Chasman			Satała			Meyer	Krieger	Bonche	
		β_2	β_4	<i>Q</i> ₀	β_2	β_4	<i>Q</i> ₀	<i>Q</i> ₀	<i>Q</i> ₀	β_2	<i>Q</i> ₀
Hg											
190	18(3) ^a	0.55	0.03	19.1	0.46	0.06	18.6	18.1		0.53	17.6 ^g 16.0 ^h
191	18(3) ^b	0.55	0.03	19.1							
192	20(2) ^c 20(3) ^d	0.55	0.03	19.2	0.48	0.07	19.9	18.2	18.0	0.54	18.5 ^g 17.5 ^h
194		0.50	0.03	19.3	0.47	0.06	19.3	18.5			
Pb											
192		0.50		17.6	0.47	0.07	19.4	18.7	17.9		
194	20(3) ^e	0.55		19.8	0.49	0.07	20.8	19.3	19.2		
196	18.3(3) ^f	0.50		17.9	0.48	0.06	20.5	19.2	20.0		
198		0.55		20.1	0.48	0.04	20.1	18.8	20.9		

^aDrigert *et al.* [10].

^bMoore *et al.* [1], Carpenter *et al.* [11].

^cMoore *et al.* [12].

^dLee *et al.* [28].

^eWillsau *et al.* [13].

^fPresent work.

^gObtained from Hartree-Fock + BCS calculations.

^hObtained from generator coordinate method calculations.

the lowest rotational frequencies. An analysis along these lines was originally proposed by Drigert *et al.* [10] who noted that, at the lowest $\hbar\omega$ values, the $\mathcal{J}^{(2)}$ curve of ^{190}Hg lies below that of either ^{192}Hg or ^{194}Hg and suggested that a somewhat smaller β_2 deformation in ^{190}Hg could be inferred. From a fit to the values of $\mathcal{J}^{(2)}$ with the Harris expression $\mathcal{J}^{(2)} = \mathcal{J}_0 + 3\mathcal{J}_1\omega^2$, one can obtain the parameter \mathcal{J}_0 which is related to the quadrupole deformation by the expression $\mathcal{J}_0 = C(Z)A^{5/3}\beta_2^2$, which follows from the Grodzins' formula [29]. In this relation, Z is the proton number, A is the nucleon number, and $C(Z)$ describes the "calibration" of the relation between \mathcal{J}_0 and β_2 . Extensive tests of this simple relation have been performed for rare earth nuclei where \mathcal{J}_0 was obtained from fits with the Harris expression and β_2 was derived from $B(E2)$ values [30]. This study showed that $C(Z)$ remains constant within an isotopic chain and varies smoothly with Z . Thus, the use of this expression in the present context seems justified.

The dynamic moments of inertia for all the SD bands in the Pb isotopes are presented as a function of $\hbar\omega$ in Fig. 5. From the figure it can be seen that at the lowest frequencies $\mathcal{J}^{(2)}$ has a lower value for ^{196}Pb and ^{198}Pb than for ^{192}Pb and ^{194}Pb . The \mathcal{J}_0 values were obtained for each Pb isotope from a least squares fit to the Harris expression over comparable frequency ranges for each band. \mathcal{J}_0 values of $88.0\hbar^2$, $89.84\hbar^2$, $87.49\hbar^2$, and $86.10\hbar^2 \text{ MeV}^{-1}$ were found for $A = 192$, 194 , 196 , and 198 , respectively. Assuming that $C(Z)$ is constant for the four SD bands, the extracted β_2 deformations would be within 0.4% in both ^{192}Pb and ^{194}Pb , but the β_2 values in ^{196}Pb and ^{198}Pb would be 2.3% and 4% smaller than in ^{194}Pb . Thus this analysis tends to corroborate the discussion given above and is consistent with the trend present in the measured Q_0 values for ^{194}Pb and ^{196}Pb , suggesting that the largest deformation occurs for ^{194}Pb . We note

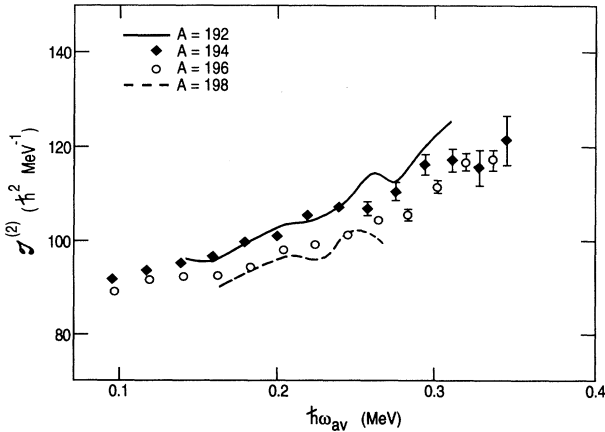


FIG. 5. Dynamic moment of inertia $\mathcal{J}^{(2)} = 4\hbar^2/\Delta E_\gamma$ for the superdeformed bands in the even Pb isotopes. The circles represent the data for ^{196}Pb and the diamonds for ^{194}Pb [14,31,32,33]. The lines represent the $\mathcal{J}^{(2)}$ curves for the superdeformed bands in ^{192}Pb [34,35] (solid) and ^{198}Pb [15] (dashed).

that in the calculations by Chasman [3] and Satuła *et al.* [5], differences of the same magnitude between ^{194}Pb and ^{196}Pb are obtained. On the other hand, these calculations do not agree as nicely with this analysis for the other two Pb isotopes.

B. Evolution of the dynamic moment of inertia with rotational frequency

In addition to the differences between the $\mathcal{J}^{(2)}$ moments of inertia described above, other interesting features emerge in Fig. 5. In all the Pb isotopes, $\mathcal{J}^{(2)}$ is rising with $\hbar\omega$ and this rise is of the same magnitude in all the isotopes up to $\hbar\omega \leq 0.3 \text{ MeV}$. This feature has been reported for a vast majority of the SD bands in the $A \sim 190$ region [2]. Above this frequency of 0.3 MeV, where data are available in the lead isotopes for only ^{194}Pb and ^{196}Pb , another interesting observation can be made: A change in the slope of the $\mathcal{J}^{(2)}$ curve is present in ^{196}Pb but not in ^{194}Pb . As a result of this change, the $\mathcal{J}^{(2)}$ values for the two isotopes become similar. The situation resembles that reported recently for the $^{190,192}\text{Hg}$ SD pair by Bearden *et al.* [36]. In these two nuclei, the $\mathcal{J}^{(2)}$ curves also exhibit similar smooth rises up to $\hbar\omega \leq 0.32 \text{ MeV}$ and, at the higher frequencies, a clear upbend in the data points is seen in ^{190}Hg only. In fact, the $\mathcal{J}^{(2)}$ values for ^{190}Hg become even larger than those for ^{192}Hg . Such a change in slope is very similar to those seen in many rotational bands at normal deformation and suggests the presence of a crossing between the SD "ground state" band and a band based on an excited configuration.

In order to try to understand these features, we have performed cranked Woods-Saxon calculations which include the effects of both static and dynamical pairing. Calculations of this type have been performed in many instances to account for the rise of $\mathcal{J}^{(2)}$ vs $\hbar\omega$ [2,37] and have attributed the observations to the alignment of $j_{15/2}$ quasineutron and $i_{13/2}$ quasiproton pairs. Strong support for this interpretation and for the role of pairing in these SD nuclei has been provided by so-called blocking experiments where the alignment of a pair of quasiparticles in odd-even or odd-odd nuclei is blocked by the presence of an odd quasiparticle in the orbital of interest (Pauli blocking). Recently, $\mathcal{J}^{(2)}$ was found to be constant with $\hbar\omega$ for two of the six SD bands in ^{192}Tl [38] and this result was interpreted in terms of Pauli blocking of quasiparticle alignments in both the $j_{15/2}$ and $i_{13/2}$ intruder orbitals.

The Woods-Saxon calculations described here for ^{194}Pb and ^{196}Pb were performed with the following parameters. The β_2 and β_4 deformation parameters were taken from Satuła *et al.* [5] (Table II) and result from self-consistent Strutinsky calculations with the same Woods-Saxon potential that is used here. The neutron and proton pairing strengths were taken to be 90% of the full pairing strength G_{full} , calculated with the particle number projection technique [26]. This choice is guided by the detailed studies presented in Ref. [10] for the ^{190}Hg

SD band and by the successful description of both normally deformed and other SD nuclei [26,39]. The calculated $\mathcal{J}^{(2)}$ moments are compared with the data in Fig. 6. From the figure, it is clear that the calculations reproduce the trends of the data rather well; i.e., at low frequency $\mathcal{J}^{(2)}$ is lower in ^{196}Pb than in ^{194}Pb , but the respective rises with frequency are such that at higher frequencies the calculations for the two nuclei result in very similar $\mathcal{J}^{(2)}$ values as seen in the data.

As in the other SD nuclei of this region, the rise in $\mathcal{J}^{(2)}$ is brought about by the alignment of a $j_{15/2}$ quasineutron and $i_{13/2}$ quasiproton pair. (Adopting the nomenclature in which SD configurations are labeled by the number of occupied intruder orbitals, the SD bands can be assigned a $\pi 6^6\nu 7^4$ configuration for both ^{194}Pb and ^{196}Pb .) The somewhat steeper slope in $\mathcal{J}^{(2)}$ calculated for ^{196}Pb originates from the interaction strength between the ground band and the aligned $j_{15/2}$ configuration, which is computed to be ~ 370 keV in ^{196}Pb and ~ 470 keV in ^{194}Pb .

It is worth pointing out that one of the problems with cranking calculations noted for Hg nuclei does not seem to occur in the calculations for the Pb isotopes. It has been shown in the case of $^{190,192}\text{Hg}$ [40,41] that the downturn of $\mathcal{J}^{(2)}$, calculated to occur at high $\hbar\omega$ after the quasiparticle alignments have taken place, is not present in the data. This failure has been interpreted as an indication that at least one of the two quasiparticle alignments is delayed in frequency and occurs with a larger interaction strength than predicted. In the cranking calculations for the Pb isotopes, the change in the Fermi surface when going from $Z = 80$ to 82 results in a delay of the $i_{13/2}$ proton crossing from $\hbar\omega \sim 0.35$ to $\hbar\omega \sim 0.55$ MeV and, as a result, the $\mathcal{J}^{(2)}$ curves continue to rise at the highest frequencies, as shown in Fig. 6.

While a consistent picture seems to emerge from these cranking calculations, it should be emphasized that they do not address some of the critical issues raised in previ-

ous work. For example, it has been suggested [10,40,41] that, in the SD bands of the Hg isotopes, the $j_{15/2}$ neutron crossing may be delayed and/or that higher order corrections to the pairing may be required to provide an adequate description of the alignment processes at very large deformations. The calculations in Fig. 6 show a small downturn in the $\mathcal{J}^{(2)}$ curves at medium frequencies which occurs after the $j_{15/2}$ quasineutrons have aligned and before the contribution due the $i_{13/2}$ quasiproton alignment becomes significant. It is possible that the absence of this effect in the data is an indication of the need for improved calculations. Also, while the magnitude of the rise in $\mathcal{J}^{(2)}$ with $\hbar\omega$ is of the right order, improved calculations might be able to follow the data more closely.

V. CONCLUSIONS

A detailed experimental study of the superdeformed band in ^{196}Pb has been performed. New transitions have been added at the top and bottom of the previously known band. The expected stretched $E2$ character of the transitions in the band has been established by the measurement of DCO ratios. The intrinsic quadrupole moment of the band has been measured using the DSAM and a value of 18.3 ± 3.0 e b was obtained. The quadrupole moment of this band and those of several other bands in the mass $A \sim 190$ region have been compared to the results of a number of theoretical calculations and were found to be consistent with a quadrupole deformation of $\beta_2 \sim 0.5$. The data suggest that the deformation reaches a maximum value for $N = 112$ in both the Hg and Pb SD bands. This trend is also present in some of the calculations. An analysis of the $\mathcal{J}^{(2)}$ behavior in the Pb SD bands corroborates the possibility of small differences in deformation between the bands.

Cranked Woods-Saxon calculations were carried out which indicate that the rise in the $\mathcal{J}^{(2)}$ values with $\hbar\omega$ is brought about by the alignment of a $j_{15/2}$ quasineutron and $i_{13/2}$ quasiproton pair. In contrast to the predictions for the SD bands in the Hg isotopes, the calculations indicate that the downturn in $\mathcal{J}^{(2)}$ following the quasiparticle alignments should occur at frequencies of $\hbar\omega \sim 0.55$ MeV, well beyond the highest experimentally observed frequencies. The differences in slope between ^{194}Pb and ^{196}Pb are attributed to different interaction strengths between the aligned $j_{15/2}$ configurations and the respective ground bands. However, in order to reproduce the $\mathcal{J}^{(2)}$ data more closely, it may be necessary to improve the calculations by including, for example, higher order corrections to pairing at large deformations.

This work was supported in part by the Department of Energy, Nuclear Physics Division under Contract Nos. DE-FG05-88ER40441, W-31-109-ENG-38, DE-AC07-76ID01570, DE-FG02-87ER4036, and by the National Science Foundation under Grant No. PHY88-02279.

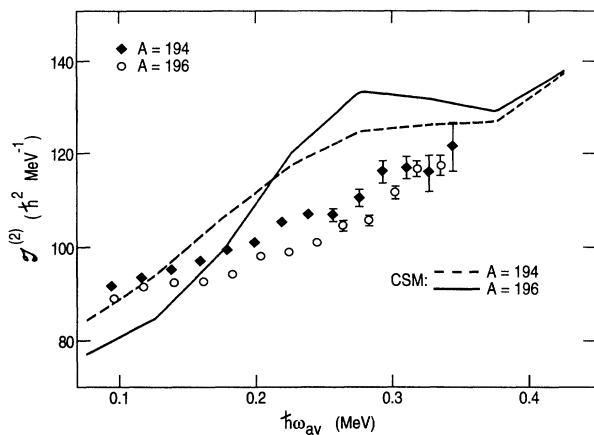


FIG. 6. Dynamic moment of inertia $\mathcal{J}^{(2)}$ as a function of rotational frequency for the superdeformed bands in ^{196}Pb (circles) and ^{194}Pb (diamonds). The calculated $\mathcal{J}^{(2)}$ curves for the SD bands in ^{196}Pb and ^{194}Pb are represented by the solid and dashed lines, respectively (see text for details).

- [1] E. F. Moore *et al.*, Phys. Rev. Lett. **63**, 360 (1989).
- [2] R. V. F. Janssens and T. L. Khoo, Annu. Rev. Part. Nucl. Sci. **41**, 321 (1991).
- [3] R. R. Chasman, Phys. Lett. B **219**, 227 (1989).
- [4] S. Åberg, Phys. Scr. **25**, 23 (1983).
- [5] W. Satulá, S. Cwiok, W. Nazarewicz, R. Wyss, and A. Johnson, Nucl. Phys. **A529**, 289 (1991).
- [6] P. Bonche, P. Quentin, S. J. Krieger, M. S. Weiss, J. Meyer, M. Meyer, N. Redon, H. Flocard, and P.-H. Heenen, Nucl. Phys. **A500**, 308 (1989).
- [7] M. Girod, J. P. Delaroche, D. Gogny, and J. F. Berger, Phys. Rev. Lett. **62**, 2452 (1989).
- [8] S. Krieger, P. Bonche, M. S. Weiss, J. Meyer, H. Flocard, and P.-H. Heenen, Nucl. Phys. **A542**, 43 (1992).
- [9] M. Meyer, N. Redon, P. Quentin, and J. Liebert, Phys. Rev. C **45**, 233 (1992).
- [10] M. W. Drigert *et al.*, Nucl. Phys. **A530**, 452 (1991).
- [11] M. P. Carpenter *et al.*, Phys. Lett. B **240**, 44 (1990).
- [12] E. F. Moore *et al.*, Phys. Rev. Lett. **64**, 3127 (1990).
- [13] P. Willsau *et al.*, Z. Phys. A **344**, 351 (1993).
- [14] M. J. Brinkman *et al.*, Z. Phys. A **336**, 115 (1990).
- [15] T. F. Wang *et al.*, Phys. Rev. C **43**, R2465 (1991).
- [16] J. R. Hughes *et al.*, Phys. Rev. C **47**, R1337 (1993).
- [17] Y. Liang *et al.* (unpublished).
- [18] E. A. Henry *et al.*, in Proceedings of the International Conference on Nuclear Structure at High Angular Momentum and Workshop on Large Gamma-Ray Detector Arrays, Ottawa, 1992 (Report No. AECL 10613, 1992), Vol. 2, p. 15.
- [19] J. J. van Ruyven *et al.*, Nucl. Phys. **A449**, 579 (1986), and references therein.
- [20] M. Piiparinen *et al.*, Phys. Lett. B **194**, 468 (1987).
- [21] H. Emling *et al.*, Phys. Lett. B **217**, 33 (1989); H. Emling *et al.*, in Proceedings of the Twenty-Second School on Physics, Zakopane, Poland, 1987, edited by R. Broda and Z. Stachura (Instytut Fizyki Jądrowej w Krakowie Report No. IFJ 1956/PL), p. 151.
- [22] J. F. Ziegler, J.P. Biersack, and U. Littmark, *The Stopping and Range of Ions in Solids* (Pergamon, New York, 1985).
- [23] H. Emling *et al.*, Nucl. Phys. **A419**, 187 (1984).
- [24] P. J. Twin *et al.*, Phys. Rev. Lett. **57**, 811 (1986).
- [25] K. E. G. Löbner, M. Vetter, and V. Hönig, Nucl. Data Sect. A **7**, 496 (1970).
- [26] W. Nazarewicz, R. Wyss, and A. Johnson, Nucl. Phys. **A503**, 285 (1989).
- [27] P. Bonche, J. Dobaczewski, H. Flocard, P.-H. Heenen, S. J. Krieger, J. Meyer, and M. S. Weiss, Nucl. Phys. **A519**, 509 (1990).
- [28] I. Y. Lee *et al.*, in [18], p. 21.
- [29] L. Grodzins, Phys. Lett. **2**, 88 (1962).
- [30] L. Zhou, L. L. Riedinger, M. P. Carpenter, and V. P. Janzen, University Tennessee Annual Report, 1988, p. 30.
- [31] K. Theine *et al.*, Z. Phys. A **336**, 113 (1990).
- [32] H. H. Hübel *et al.*, Nucl. Phys. **A520**, 125c (1990).
- [33] F. Hannachi *et al.*, in [18], p. 384.
- [34] E. A. Henry *et al.*, Z. Phys. A **338**, 469 (1991).
- [35] A. J. M. Plompen *et al.*, Phys. Rev. C **47**, 2378 (1993).
- [36] I. G. Bearden *et al.*, in [18], p. 10.
- [37] M. A. Riley *et al.*, Nucl. Phys. **A512**, 178 (1990).
- [38] Y. Liang *et al.*, Phys. Rev. C **46**, R2136 (1992).
- [39] B. D. Kern *et al.*, Phys. Rev. C **36**, 1514 (1987).
- [40] I. G. Bearden *et al.*, Z. Phys. A **341**, 491 (1992).
- [41] T. Lauritsen *et al.*, Phys. Lett. B **279**, 239 (1992).